Available online at www.sciencedirect.com
ScienceDirect
Trans. Nonferrous Met. Soc. China 31(2021) 1993−2004
Transactions of Nonferrous Metals Society of China
www.tnmsc.cn

Quantitative characterization of β-solidifying γ-TiAl alloy with duplex structure

Run-run XU, Miao-quan LI

School of Materials Science and Engineering, Northwestern Polytechnical University, Xi'an 710072, China

Received 24 July 2020; accepted 9 April 2021

Abstract: For precise plastic deformation, microstructure control is essential especially for β-solidifying γ-TiAl alloy with duplex structure. Based on stereology, the microstructure of isothermally compressed γ-TiAl alloy was divided into β_0 grains, remnant α_2/γ lamellar colonies, α_2 and γ grains. The results show that the volume fraction of β_0 grains slightly increases in the isothermally compressed γ-TiAl alloy with the increase of height reduction. Meanwhile, the volume fractions of remnant α_2/γ lamellar colonies and α_2 grains decrease. However, the volume fraction of γ grains increases from 64.39% to 78.47%. According to the quantitative results, the $\alpha\rightarrow\gamma$ phase transformation was investigated in-depth, and it is found that isothermal compression accelerates the $\alpha\rightarrow\gamma$ phase transformation. The first $\alpha\rightarrow\gamma$ phase transformation is similar to ledge-controlled transformation, through which remnant α_2/γ lamellar colonies finally convert into γ grains in isothermal compression. The second is achieved by α/γ phase interface immigration.
Key words: TiAl alloy; stereology; digital image analysis; microstructure; phase transformation

1 Introduction

In recent years, weight-saving becomes a crucial issue for improving the fuel efficiency and service performance of aircraft engines. The first way out is advanced design. For example, PRATT & WHITNEY Company replaced conventional jet engines with PW1100G-JM engines, in which a speed-reduction gearbox was introduced to increase the bypass ratio [1]. The second solution is substituting light-weight alloys for heavy Ni-based alloys. Since 2006, γ-TiAl alloys with the density of 3.9−4.2 g/cm^3 have been widely used as low-pressure turbine blades in aero engines like GEnx engines, resulting in a weight saving of about 400 lbs [2,3]. So far, the components of γ-TiAl alloys after thermomechanical processing have been successfully implemented in aero engines, and the performance of γ-TiAl alloys is strongly related to internal microstructure characteristics [4−6].

To achieve microstructure control, intensive researches were focused on microstructure evolutions like dynamic recrystallization (DRX) and phase transformations in thermomechanical processing of γ-TiAl alloys [7−9]. ZHANG et al [10] investigated the mechanisms of Ti−43Al−9V−0.2Y (at.%, hereafter) hot-rolled above α-transus temperature. XIANG et al [11] acclaimed that DRX induced by twinning and $\alpha_2\rightarrow\beta$ phase transformation occurred in the isothermal compression of TNM alloys. SOKOLOVSKY et al [12] found that deformation assisted $\gamma\rightarrow\alpha$ phase transformation when Ti−43.2Al−1.9V−1.1Nb−1.0Zr was hot compressed in (α+γ) phase field. ZONG et al [13] claimed that hydrogen promoted $\alpha_2\rightarrow B2$ phase transformation and α_2 lamellae coarsening. Previous studies [14−17] were focused on precipitation of γ lamellae via $\alpha/\alpha_2\rightarrow\gamma$ phase transformation during the cooling of γ-TiAl

Corresponding author: Miao-quan LI, Tel: +86-29-88460328, E-mail: honeymli@nwpu.edu.cn
DOI: 10.1016/S1003-6326(21)65632-7

alloys, while the $\alpha \rightarrow \gamma$ phase transformation in isothermal compression is less concerned. In most cases, multiple phases coexist in γ-TiAl alloys, which perhaps affect phase transformation mechanisms. So, it is obliged for the quantitative characterization of multi-phase γ-TiAl alloys. In Ref. [18], quantitative analysis was carried out for microstructure characteristics of TNM alloy heat treated under various conditions by SEM and XRD. However, unreasonable results of volume fractions perhaps appear for combining two technologies. Moreover, previous studies [18,19] neglected the distribution and the orientation uniformity for the microstructure of γ-TiAl alloys.

In this work, quantitative characterization was carried out for Ti−42.9Al−4.6Nb−2Cr with duplex structure after isothermal compression. Four types of characteristic parameters were measured and presented as the functions of height reduction to elucidate the influence of deformation. According to quantitative analysis, the phase transformation mechanisms of the isothermally compressed Ti−42.9Al−4.6Nb−2Cr were investigated via TEM technology. Such quantitative characterization is important to establish constitutive models and comprehensively evaluate the microstructure of multi-phase γ-TiAl alloys.

2 Experiments and digital image separation

Ti−42.9Al−4.6Nb−2Cr, a commercial β-solidifying γ-TiAl alloy with duplex structure, was supplied in the present study. As seen from Fig. 1(a), the starting microstructure of Ti−42.9Al−4.6Nb−2Cr consists of the elongated β_0 grains, equiaxed γ grains and α_2/γ lamellar colonies. The α-transus temperature of Ti−42.9Al−4.6Nb−2Cr was approximately 1281 °C.

The as-received Ti−42.9Al−4.6Nb−2Cr billet was manufactured into cylinders with a diameter of 8 mm and a height of 12 mm. Isothermal compression tests were performed on the Thermecmastor-Z thermomechanical simulator at a deformation temperature of 1200 °C and strain rate of 0.01 s^{-1}, and the height reductions of 20%−50% in vacuum. Details of isothermal compression tests were described in Refs. [20,21]. Isothermally compressed specimens were sectioned axially, and then mechanically ground to 1500 grit for electro-polishing. After electro-polishing, specimens were observed on an FEI Helios G4 CX SEM in back-scattered electron (BSE) mode. All observations were taken from large deformation areas of deformed specimens.

Figure 1(b) shows the SEM-BSE image of the isothermally compressed Ti−42.9Al−4.6Nb−2Cr. As seen from Fig. 1(b), the microstructure of Ti−42.9Al−4.6Nb−2Cr after compression was composed of remnant α_2/γ lamellar colonies partly with kinked characteristic, β_0 phase with the highest contrast, newly-formed γ grains, and some α_2 grains which were new α_2/γ lamellar colonies formed during subsequent air-cooling. Hereafter, the newly formed α_2/γ lamellar colonies were termed as α_2 grains. EBSD data were collected via a TESCAN MIRA3 XMU SEM and NordlysMax detector. After that, Schmid factors were calculated via HKL Channel5 software. The nanoscale observation was performed on an FEI Talos F200X TEM.

A seamless montage was created by nine SEM−BSE images with high resolution, to avoid the local non-uniform distribution of microstructure and ensure the reliability of quantitative characterization. According to plastic deformation

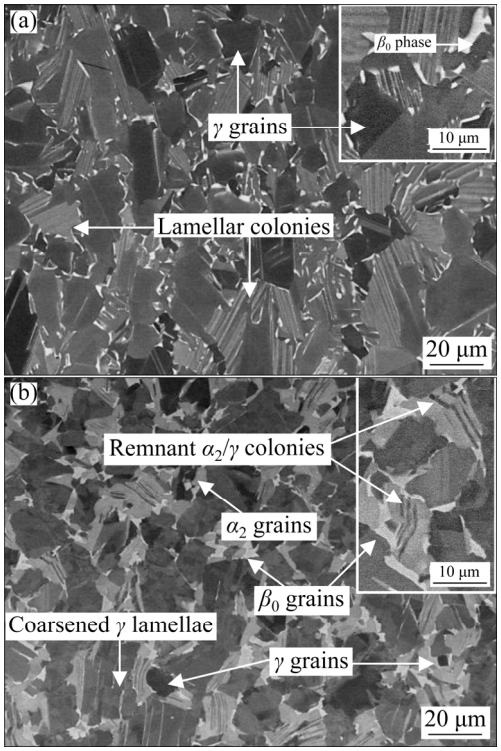

Fig. 1 SEM images of initial Ti−42.9Al−4.6Nb−2Cr (a) and isothermally compressed Ti−42.9Al−4.6Nb−2Cr at 1200 °C and strain rate of 0.01 s^{-1} with height reduction of 20% (b)

behavior, the microstructure of Ti−42.9Al−4.6Nb−2Cr after isothermal compression was divided into four units, β_0 grains, remnant α_2/γ lamellar colonies, α_2 and γ grains. The content of backscattered electrons is linked to atomic number, so γ, α_2 and β_0 phases present various gray values and can be effectively distinguished on SEM-BSE images. However, all automatic segmentation technologies based on gray value variation were failed to distinguish four units in β-solidifying γ-TiAl alloys. Thereby, SEM-BSE images were manually segmented.

3 Characterization parameters

According to the stereology and metallography, four characteristic parameters (volume fraction, size parameters, distribution parameters and orientation parameters) were chosen to describe the microstructure morphology. The measurement of characteristic parameters was carried out via Image-Pro Plus version 6.0 software. According to Dellesse law, the volume fraction of structural units is the sum of object areas divided by image areas. In the present work, the volume fractions of γ grains in as-received or compressed Ti−42.9Al−4.6Nb−2Cr were higher than 60%, and most γ grains were adhered with each other, which would seriously deteriorate the quantitative accuracy of γ grains. Therefore, other characteristic parameters are targeted for α_2/γ lamellar colonies, β_0 and α_2 grains.

3.1 Size parameters

3.1.1 Sizes of grains or lamellar colonies

In the present work, the average grain intercept method was adopted. For accurate measurement, lines passing through the object's centroid were rotated with an angle of 2°, as shown in Fig. 2. And each dimension of objects was calculated by the average length of intercepted lines l_k. Then, the average dimension of grains or lamellar colonies was equal to the sum of dimensions divided by the numbers of measured objects.

3.1.2 Shape factor

The aspect ratio was adopted to describe the morphological alteration of regular grains and α_2/γ lamellar colonies, and is expressed as follows:

$$s=l_{max}/l_{min} \quad (1)$$

where l_{max} and l_{min} represent the length (μm) for the major and minor axes of the fitting ellipse (which is equivalent to the object with the same area), and s is the aspect ratio of measured objects. The larger the shape factor is, the closer the shape of the object to circle is.

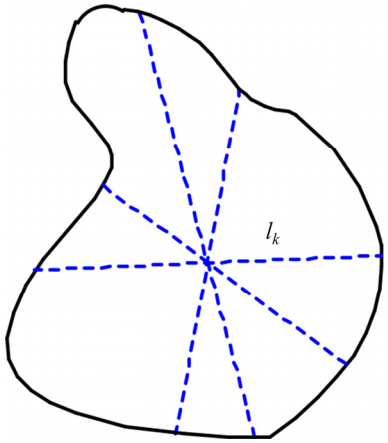

Fig. 2 Schematic diagram for lamellar colonies/grain size of measured objects

As seen from Fig. 1(b), some β_0 grains are elongated and present serrated edges, implying that the aspect ratio might be less effective for these irregular grains, especially for those with W-shape or O-shape. In light of the aforementioned cases, the roundness (r) instead of aspect ratio was used to manifest the variation of β_0 grains, and is calculated by the following equation:

$$r=P^2/(4\pi A) \quad (2)$$

where P and A are the perimeter (μm) and area (μm^2) of the measured object, respectively. For round particles with the radius of a, the perimeter and area are $2\pi a$ and πa^2, respectively. And the calculated roundness r is 1. Since the roundness and aspect ratio show similar variation tendency, the aspect ratio was preserved to describe shape change for other grains and α_2/γ lamellar colonies.

3.1.3 Lamellar spacing

Concerning the sandwiched structure, the layer thickness is one of the essential parameters related to mechanical properties, like yield strength. Therefore, the lamellar thickness should be included in the quantitative characterization of α_2/γ lamellar colonies. To be clear, the γ/γ interface between γ variants is a twin interface, and intensive γ domains with twin orientations coexist in a single γ variant. Thereby, the distance between α_2/γ

interfaces was adopted as lamellar spacing. As the present work was focused on the effect of height reduction, the lamellar spacing of newly-formed α_2/γ lamellar colonies (α_2 grains) was omitted, since these lamellar colonies were formed after isothermal compression.

3.2 Distribution parameters

The spatial arrangement homogeneity of structural units is indispensable for microstructure quantification. From the scene in Fig. 3, Points *C* and *D* tied with elastic band move along edges of islands *A* and *B*, respectively. Then, the distance between islands *A* and *B* equals the mean length of the elastic band. This means that the distribution of particles can be quantified by mean free path λ, which is given by [22]

$$\lambda=(1-V_V)/N_L \tag{3}$$

where V_V is the volume fraction (%) of the measured object, N_L represents the possibility that line segment in per unit length (termed as L_0 hereafter) encounters measured objects, or the crossing number when L_0 intersects with the edge of measured objects.

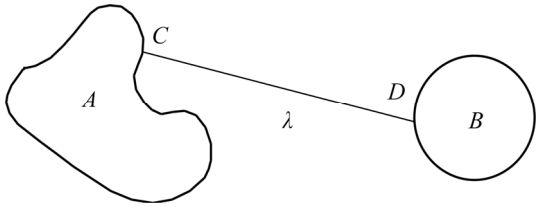

Fig. 3 Illustration of mean free path λ

Referring to CHEN et al [23], Eq. (3) can be calculated via other stereographic parameters, and the relationship is

$$\lambda=2\left(1-V_V\right)\sqrt{D_{max}D_{min}}\,/\,3V_V \tag{4}$$

where D_{max} and D_{min} represent the maximum and minimum diameters (μm) of measured object, respectively. As β_0 grains distributed as necklace-structure along α_2/γ lamellar colonies and γ grains, D_{max} and D_{min} in Eq. (4) were replaced by l_{max} and l_{min} for high quantitative accuracy.

For rod-shaped microstructure units, the angle θ_1 between the major axis of the fitting ellipse and compression direction was also adopted to describe the distribution homogeneity for microstructure, as illustrated in Fig. 4.

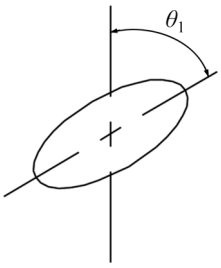

Fig. 4 Characteristic parameter θ_1 for distribution

3.3 Orientation parameters

γ and α_2 lamellae kept Blackburn crystallographic orientation relationship as $\{111\}_\gamma//(0001)_{\alpha_2}$ and $\langle 1\bar{1}0\rangle_\gamma//\langle 11\bar{2}0\rangle_{\alpha_2}$ [24]. Most often, deformation of γ lamellae occurs on {111} close-packed planes, while that of α_2 lamellae only happens when the compression axis is perpendicular to ⟨0001⟩ axis, leading to large deformation anisotropy of α_2/γ lamellar colonies [25,26]. Considering that, the angle θ_2 between the lamellar interface (α_2/γ phase interface) and compression axis was involved in quantitative characterization, and is illustrated in Fig. 5.

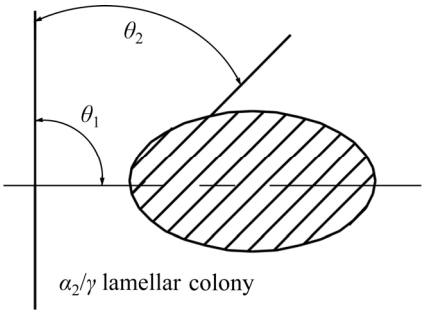

Fig. 5 Characteristic parameter θ_2 for orientation of α_2/γ lamellar colony

4 Results and discussion

4.1 Microstructure characteristics of β_0 grains

Figure 6 shows the variation of characteristic parameters for β_0 grains of the isothermally compressed Ti−42.9Al−4.6Nb−2Cr at deformation temperature of 1200 °C and strain rate of 0.01 s^{-1}. As seen from Figs. 6(a, b), the volume fraction slightly increases, while the grain size of β_0 grains in the isothermally compressed Ti−42.9Al−4.6Nb−2Cr changes in volatility with the increase of height reductions from 20% to 50%. And the average volume fraction and grain size of β_0 grains

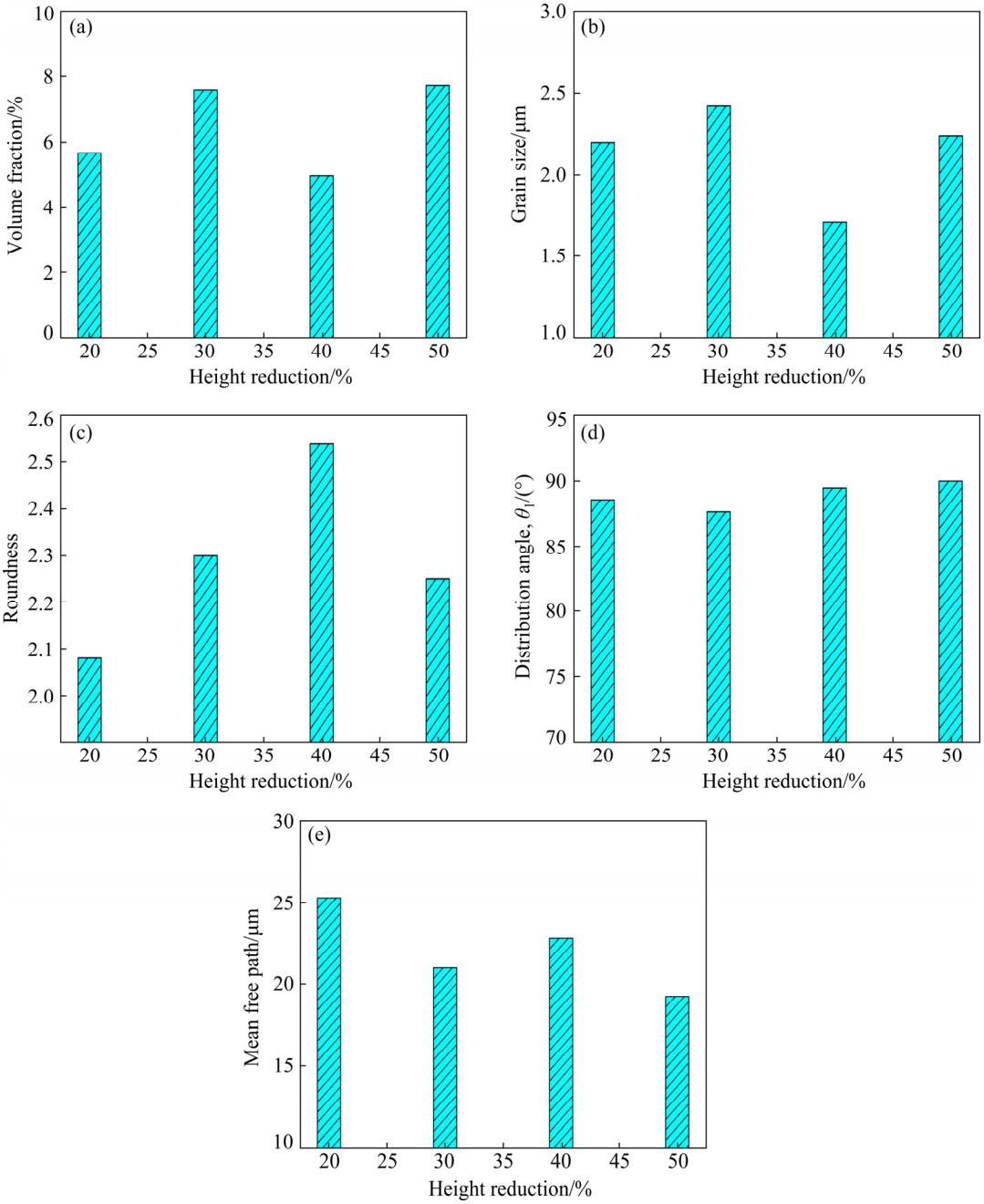

Fig. 6 Effect of height reduction on characteristic parameters of β_0 grains in isothermally compressed Ti−42.9Al−4.6Nb−2Cr at 1200 °C and 0.01 s^{-1}: (a) Volume fraction; (b) Grain size; (c) Roundness; (d) Distribution angle; (e) Mean free path

are 6.50% and 2.14 μm, respectively. As seen from Fig. 6(c), the roundness of β_0 grains in the isothermally compressed Ti−42.9Al−4.6Nb−2Cr decreases after an increase with increasing height reduction, reaching the maximum roundness (2.54) at a height reduction of 40%. As seen from Fig. 6(d), the height reduction has a slight impact on the distribution angle θ_1 in the isothermally compressed Ti−42.9Al−4.6Nb−2Cr, and the average angle θ_1 is about 89.06°. With the increase of height reduction, the mean free path of β_0 grains in the isothermally compressed Ti−42.9Al−4.6Nb−2Cr decreases (Fig. 6(e)). Such variations indicate that the distribution heterogeneity for β_0 grains increases in the isothermal compression of Ti−42.9Al−4.6Nb−2Cr, and the changes might be relevant to grain evolution behavior of other phase or deformation-induced phase transformation.

4.2 Microstructure characteristics of remnant α_2/γ lamellar colonies

Figure 7 exhibits the variation of remnant α_2/γ lamellar colonies in the isothermal compression of Ti−42.9Al−4.6Nb−2Cr. As seen from Fig. 7(a), the volume fraction decreases with the increase of height reduction. And the size of remnant α_2/γ lamellar colonies in the isothermally compressed

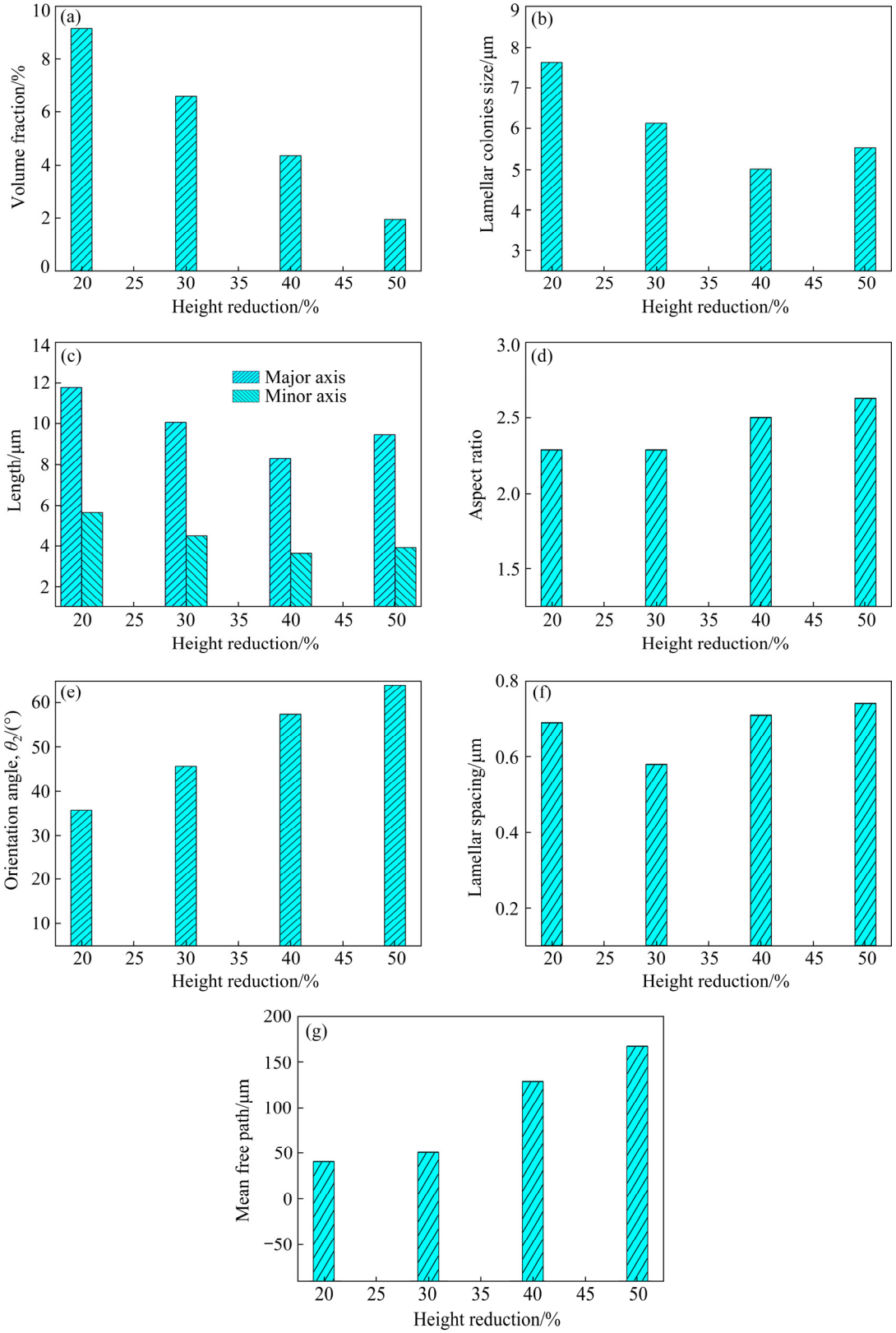

Fig. 7 Effect of height reduction on characteristic parameters of remnant α_2/γ lamellar colonies in isothermally compressed Ti−42.9Al−4.6Nb−2Cr at 1200 °C and 0.01 s^{-1}: (a) Volume fraction [27]; (b) Lamellar colonies size; (c) Length of fitting ellipse; (d) Aspect ratio; (e) Orientation angle, θ_2; (f) Lamellar spacing; (g) Mean free path

Ti−42.9Al−4.6Nb−2Cr decreases from 7.62 to 5.52 μm (Fig. 7(b)). Meanwhile, the length of major axis decreases from 11.78 to 9.45 μm, and the length of minor axis decreases from 5.64 to 3.92 μm, whereas the aspect ratio increases from 2.29 to 2.63, as shown in Figs. 7(c, d). These changes indicate that remnant α_2/γ lamellar colonies of Ti−42.9Al−4.6Nb−2Cr are gradually consumed by other structural units in isothermal compression. As seen from Fig. 7(e), the orientation angle θ_2 between the α_2/γ phase interface and the compression axis in the isothermally compressed Ti−42.9Al−4.6Nb−2Cr increases from 35.77° to 63.99° with the increase of height reduction, implying a significant reduction in remnant α_2/γ lamellar colonies with the orientation range of 0°−45° to the compression axis. Moreover, the lamellar spacing, which is the distance of α_2/γ phase interface in remnant α_2/γ lamellar colonies for the isothermally compressed Ti−42.9Al−4.6Nb−2Cr, increases slightly from 0.69 to 0.74 μm (Fig. 7(f)). The mean free path of remnant α_2/γ lamellar colonies in the isothermally compressed Ti−42.9Al−4.6Nb−2Cr increases (Fig. 7(g)), implying that the distance of remnant α_2/γ lamellar colonies increases as the height reduction increases.

4.3 Microstructure characteristics of α_2 grains

Figure 8 presents the quantitative variations of α_2 grains (α_2/γ lamellar colonies newly-formed in

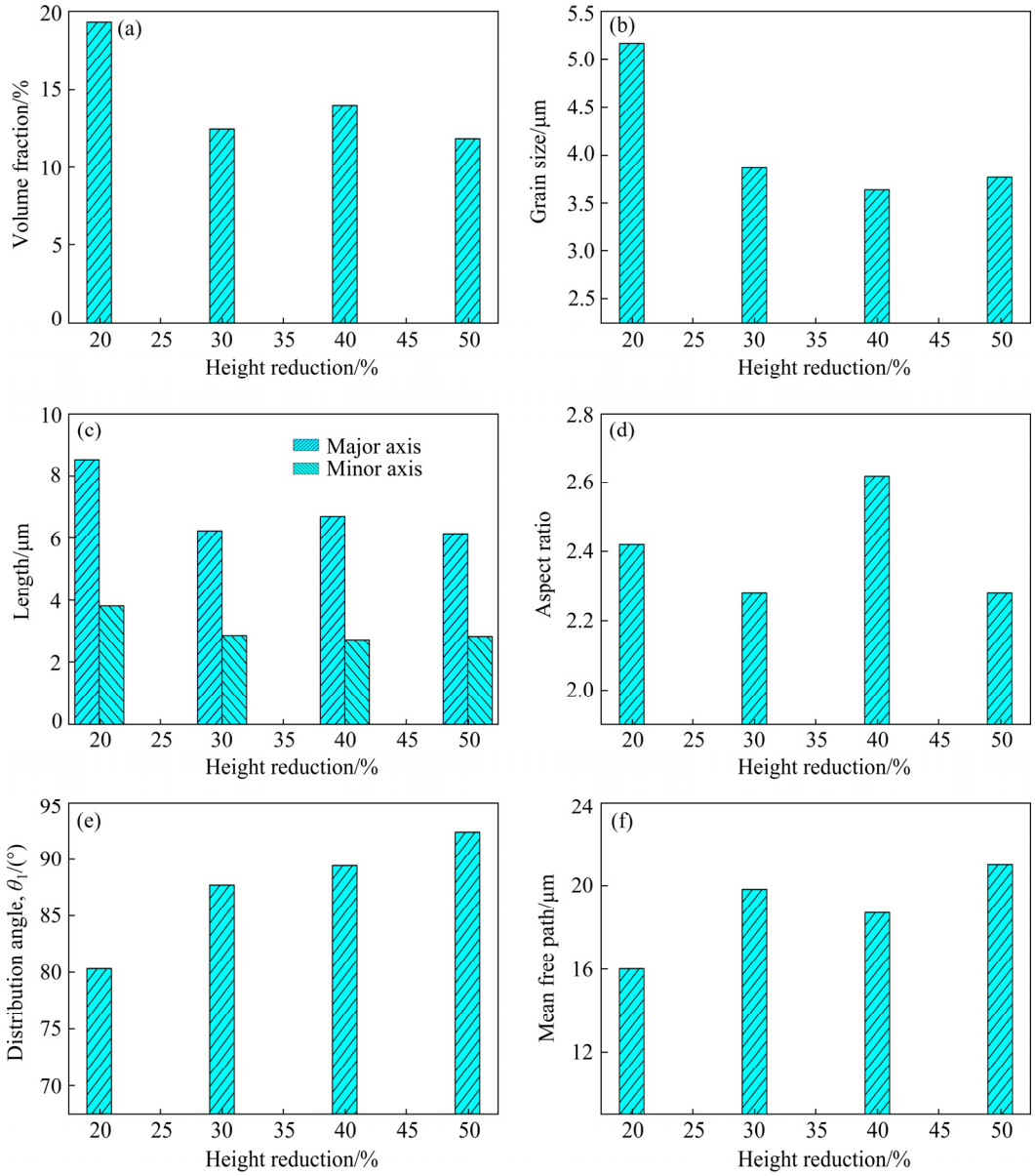

Fig. 8 Effect of height reduction on characteristic parameters of α_2 grains in isothermally compressed Ti−42.9Al−4.6Nb−2Cr at 1200 °C and 0.01 s^{-1}: (a) Volume fraction; (b) Grain size; (c) Length of fitting ellipse; (d) Aspect ratio; (e) Distribution angle, θ_1; (f) Mean free path

subsequent air-cooling) of isothermally compressed Ti−42.9Al−4.6Nb−2Cr. The volume fraction of α_2 grains in the isothermally compressed Ti−42.9Al−4.6Nb−2Cr decreases from 19.32% to 11.84%, and the grain size decreases from 5.17 to 3.64 μm with the increase of height reduction, as seen from Figs. 8(a, b). Howbeit lengths of major and minor axis decrease from 8.52 and 3.81 μm to 6.68 and 2.72 μm (Fig. 8(c)), respectively, and the aspect ratio presents a wave change as the height reduction increases from 20% to 50% (Fig. 8(d)). Meanwhile, the distribution angle θ_1 and mean free length of α_2 grains increase, as seen from Figs. 8(e, f). And the maximum value of mean free length is 21.03 μm.

4.4 Microstructure characteristics of γ grains

Figure 9 presents the volume fraction of γ grains for the isothermally compressed Ti−42.9Al−4.6Nb−2Cr at deformation temperature of 1200 °C and strain rate of 0.01 s^{-1} with height reduction of 20%−50%. As interpreted in Section 3, it is technically unfeasible to measure other characteristic parameters of γ grains. As seen from Fig. 9, the volume fraction of γ grains in the isothermally compressed Ti−42.9Al−4.6Nb−2Cr increases from 64.39% to 78.47% with the increase of height reduction. By combining with Figs. 6(a), 7(a) and 8(a), it can be inferred that the increase in γ grains of the isothermally compressed Ti−42.9Al−4.6Nb−2Cr is relative to the decrease of remnant α_2/γ lamellar colonies and α grains. This shows that isothermal compression promotes the $\alpha\rightarrow\gamma$ phase transformation in the isothermally compressed Ti−42.9Al−4.6Nb−2Cr with duplex structure.

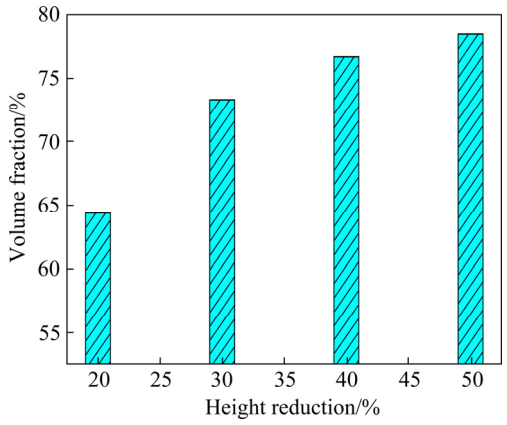

Fig. 9 Effect of height reduction on volume fraction of γ grains in isothermally compressed Ti−42.9Al−4.6Nb−2Cr at 1200 °C and 0.01 s^{-1}.

4.5 $\alpha\rightarrow\gamma$ phase transformation

4.5.1 Distribution of Schmid factor

According to the previous results [24,28,29], main deformation systems in the γ phase are $1/2\langle 1\bar{1}0\rangle\{111\}$ and $1/6\langle 11\bar{2}\rangle\{111\}$, and main potential systems in α_2 phase are $1/3\langle 11\bar{2}0\rangle\{10\bar{1}0\}$ and $1/3\langle 11\bar{2}0\rangle(0001)$. Figure 10 presents the distribution histograms of Schmid factor for γ and α_2 phase of the isothermally compressed Ti−42.9Al−4.6Nb−2Cr at deformation temperature of 1200 °C and strain rate of 0.01 s^{-1} with height reduction of 40%. As seen from Fig. 10(a), proportions of Schmid factor (m>0.25) for ordinary dislocations slip and twinning systems in γ phase are 89.17% and 72.45%, respectively, which means that most γ phase is in favorable orientations for compression. For the α_2 phase, fractions for basal and prismatic slip systems are 70.47% and 57.55%, respectively. According to the results in Ref. [28], the critical resolved shear stress (CRSS) for basal slip is three times higher than the CRSS for

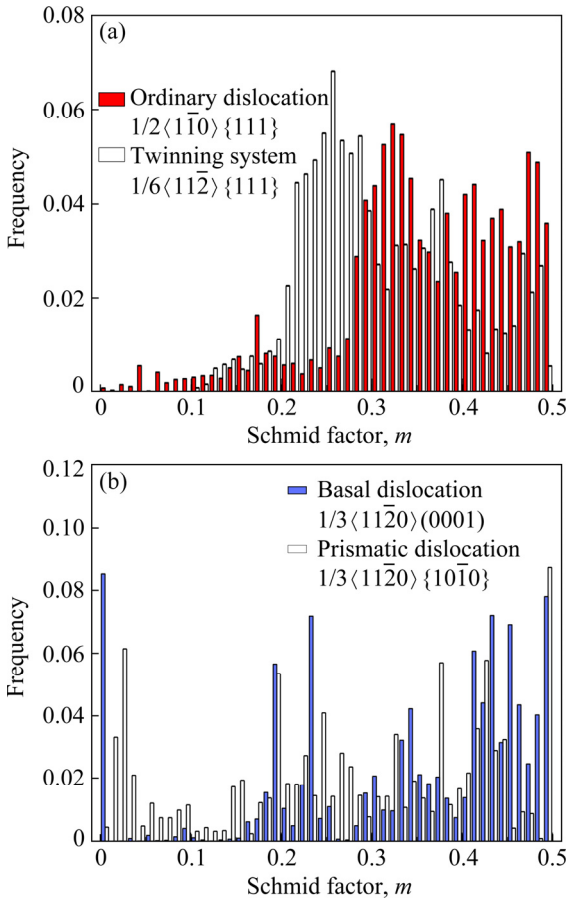

Fig. 10 Distribution histograms of Schmid factor for γ (a) and α (b) phases in isothermally compressed Ti−42.9Al−4.6Nb−2Cr at 1200 °C and strain rate of 0.01 s^{-1} with height reduction of 40%

prismatic slip. Thus, it can be inferred that a considerable number of α_2 phase is unfavorable for plastic deformation. Therefore, intensive dislocations are blocked at the α_2/γ interfaces, which might facilitate $\alpha\rightarrow\gamma$ phase transformation in the isothermal compression of Ti−42.9Al−4.6Nb−2Cr.

4.5.2 $\alpha\rightarrow\gamma$ phase transformation during isothermal compression

Figure 11 presents TEM images and element distributions of the isothermally compressed Ti−42.9Al−4.6Nb−2Cr at deformation temperature of 1200 °C and strain rate of 0.01 s^{-1}, with height reductions of 40%−50%. As seen from Figs. 11(a, b), significant dislocations are activated in γ lamellae of the isothermally compressed Ti−42.9Al−4.6Nb−2Cr, while fewer dislocations are observed in α_2 lamellae, which is consistent with analysis in Section 4.5.1. Moreover, γ lamellae, which are confirmed by SEAD pattern in the insert of Fig. 11(a) and element distributions in Figs. 11(c−f), grow into a wedge-shaped morphology by consumption of α_2 lamellae. Such an $\alpha\rightarrow\gamma$ phase transformation in the isothermal compression is less reported and is different from the $\alpha/\alpha_2\rightarrow\gamma$ phase transformation in subsequent air-cooling of Ti−42.9Al−4.6Nb−2Cr. In terms of the solidification theory [30], the $\alpha\rightarrow\gamma$ phase transformation in Figs. 11(a, b) is analogous to the ledge-controlled transformation with the aid of spiral dislocations. Due to fewer dislocations in α_2 lamellae, it can be inferred that this phase transformation is induced by accumulated stress at α_2/γ phase interface, and is significantly promoted by isothermal compression instead of elements diffusion. Consequently, γ lamellae would convert into γ grains. Moreover, as seen from the dotted box of Fig. 11(b), γ grain bows into α_2/γ lamellar colony, indicating that this $\alpha\rightarrow\gamma$ phase transformation is achieved by α_2/γ phase interface immigration.

4.5.3 $\alpha/\alpha_2\rightarrow\gamma$ phase transformation in subsequent air-cooling

Figure 12(a) shows the precipitation of γ nano-twins and γ lamellae in α_2 phase of the isothermally compressed Ti−42.9Al−4.6Nb−2Cr at deformation temperature of 1200 °C and strain rate of 0.01 s^{-1}, with height reduction of 20%. Figure 12(b) presents the selected HRTEM image. As seen from Fig. 12(a), significant amount of precipitates with varied thickness arrange in a row, indicating that

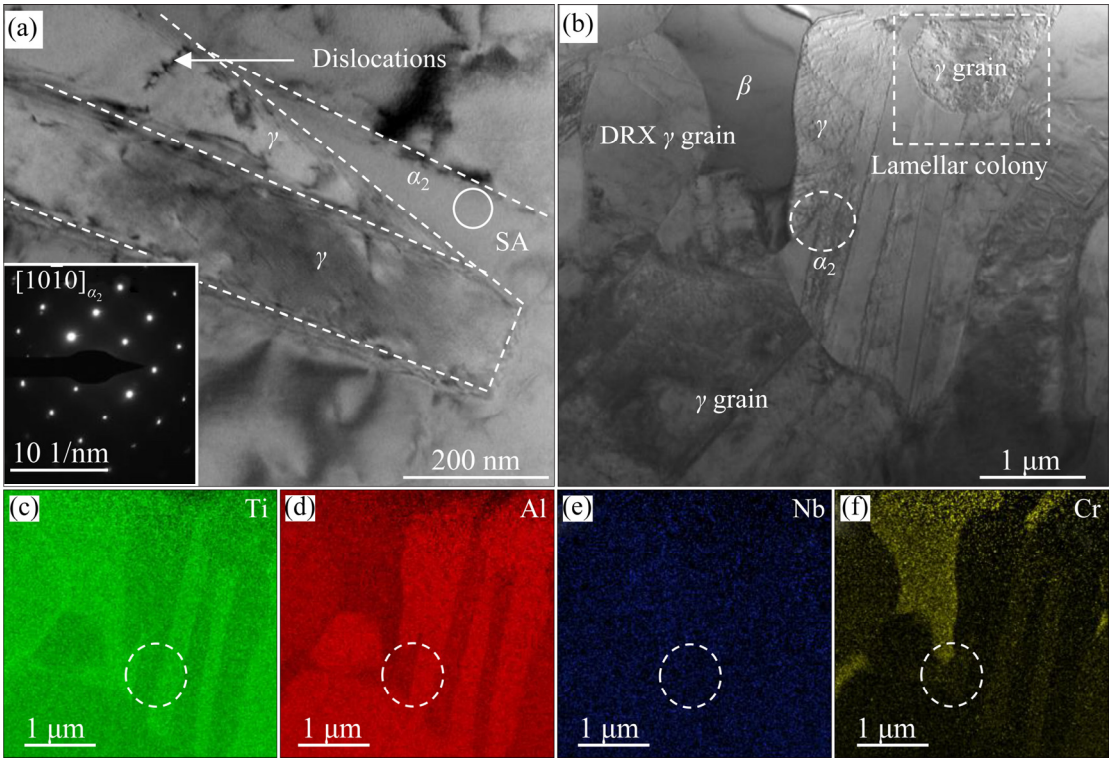

Fig. 11 TEM images of Ti−42.9Al−4.6Nb−2Cr isothermally compressed at 1200 °C and strain rate of 0.01 s^{-1} with different height reductions: (a) 40%; (b) 50%; (c−f) Elements distributions of (b) (The insert in (a) is the corresponding SAED pattern of SA)

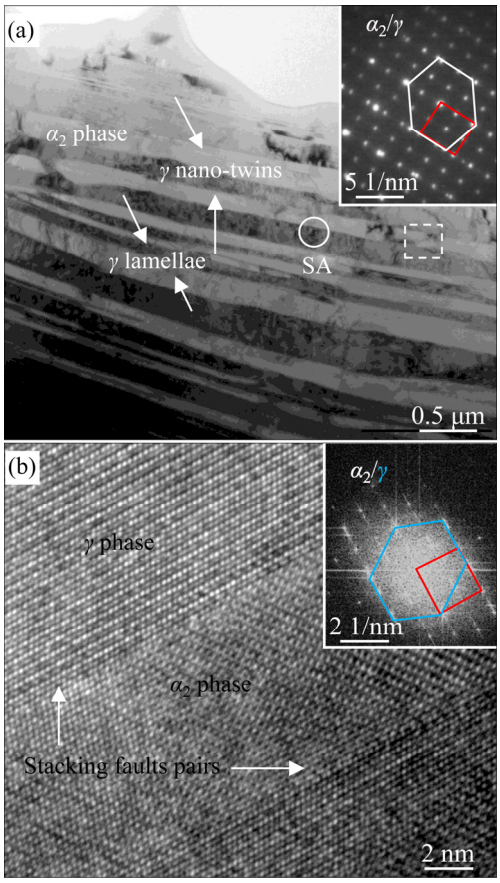

Fig. 12 TEM (a) and HRTEM (b) images of Ti−42.9Al−4.6Nb−2Cr isothermally compressed at 1200 °C and strain rate of 0.01 s^{-1} with height reduction of 20%

the precipitation is in a specific direction. From a nanoscale observation (Fig. 12(b)), γ lamellae in the isothermally compressed Ti−42.9Al−4.6Nb−2Cr consist of intensive nano-twins. Indeed, these γ nano-twins are multiple layers of superlattice intrinsic stacking fault (SISF) produced by Shockley partial dislocations [31]. Therefore, the $\alpha/\alpha_2\rightarrow\gamma$ phase transformation in the isothermally compressed Ti−42.9Al−4.6Nb−2Cr in Fig. 12 is achieved by the motion of Shockley partial dislocations. This phase transformation is achieved without the aid of phase interface immigration, and it could be speculated that this $\alpha/\alpha_2\rightarrow\gamma$ phase transformation occurred during subsequent air-cooling. As for the present cooling rate (700 °C/min), atom diffusion contributes little for $\alpha/\alpha_2\rightarrow\gamma$ phase transformation. DEY et al [14] reported similar $\alpha/\alpha_2\rightarrow\gamma$ phase transformation via continuous nucleation occurred during fast cooling of Ti−46.8Al−1.7Cr−1.8Nb. Considering that the $\alpha\rightarrow\alpha_2$ ordering would happen in air-cooling and some γ lamellae would also precipitate from the α_2 phase, the phase transformation in Fig. 12 cannot be limited to the $\alpha\rightarrow\gamma$ phase transformation.

5 Conclusions

(1) The volume fraction of β_0 grains slightly increases in the isothermally compressed Ti−42.9Al−4.6Nb−2Cr with the increase of height reduction. Meanwhile, the mean free length increases. However, the height reduction plays a little role in the distribution angle θ_1 (the angle between the major axis and compression axis), and the average value for θ_1 is 89.06°.

(2) The volume fraction and lamellar colonies size decrease with the increase of height reduction. Conversely, the orientation angle θ_2 between the α_2/γ phase interface and compression axis, spacing distance of α_2/γ phase interfaces and mean free path of remnant α_2/γ lamellar colonies increase with the increase of height reduction.

(3) The volume fraction, grain size, lengths of major and minor axis for α_2 grains decrease with the increase of height reduction, whereas the mean free length increases. Meanwhile, the volume fraction of γ grains increases from 64.39% to 78.47%.

(4) Three types of $\alpha\rightarrow\gamma$ phase transformation mechanisms occur in the isothermally compressed Ti−42.9Al−4.6Nb−2Cr. The first one is analogous to the ledge-controlled transformation induced by isothermal compression, the second is achieved by α/γ phase interface immigration and the third is formed by the coalescence of stacking faults pairs in subsequent air-cooling.

Acknowledgments

The authors are grateful for the financial supports from the National Natural Science Foundation of China (No. 51975478), and the Fundamental Research Funds for the Central Universities, China (No. 3102019MS0403).

References

[1] MAYER S, ERDELY P, FISCHER F D, HOLEC D, KASTENHUBER M, KLEIN T, CLEMENS H. Intermetallic β-solidifying γ-TiAl based alloys − From fundamental research to application [J]. Advanced Engineering Materials, 2017, 19(4): 1600735.

[2] GE Aviation. https://www.geaviation.com/commercial/engines/genx-engine, 2021−05−29.

[3] BEWLAY B P, NAG S, SUZUKI A, WEIMER M J. TiAl

alloys in commercial aircraft engines [J]. High Temperature Technology, 2016, 33(4−5): 549−559.

[4] CLEMENS H, MAYER S. Design, processing, microstructure, properties, and applications of advanced intermetallic TiAl alloys [J]. Advanced Engineering Materials, 2013, 15(4): 191−215.

[5] JIA Yi, LIU Zhi-dong, LI Sha, YAO Hao-ming, REN Zhong-kai, WANG Tao, HAN Jian-chao, XIAO Shu-long, CHEN Yu-yong. Effect of cooling rate on solidification microstructure and mechanical properties of TiB_2-containing TiAl alloy [J]. Transactions of Nonferrous Metals Society of China, 2021, 31(2): 391−403.

[6] ISMAEEL A, WANG Cun-shan. Effect of Nb additions on microstructure and properties of γ-TiAl based alloys fabricated by selective laser melting [J]. Transactions of Nonferrous Metals Society of China, 2019, 29(5): 1007−1016.

[7] LI Jian-bo, LIU Yong, WANG Yan, LIU Bin, HE Yue-hui. Dynamic recrystallization behavior of an as-cast TiAl alloy during hot compression [J]. Materials Characterization, 2014, 97: 169−177.

[8] WANG Gang, XU Lei, TIAN Yu-xing, ZHENG Zhuo, CUI Yu-you, YANG Rui. Flow behavior and microstructure evolution of a P/M TiAl alloy during high temperature deformation [J]. Materials Science and Engineering A, 2011, 528: 6754−6763.

[9] CUI Ning, KONG Fan-tao, WANG Xiao-peng, CHEN Yu-yong, ZHOU Hai-tao. Hot deformation behavior and dynamic recrystallization of a β-solidifying TiAl alloy [J]. Materials Science and Engineering A, 2015, 652: 231−238.

[10] ZHANG Yu, WANG Xiao-peng, KONG Fan-tao, SUN Liang-liang, CHEN Yu-yong. A high-performance β-solidifying TiAl alloy sheet: Multi-type lamellar microstructure and phase transformation [J]. Materials Characterization, 2018, 138: 136−144.

[11] XIANG Lin, TANG Bin, XUE Xiang-yi, KOU Hong-chao, LI Jin-shan. Microstructural characteristics and dynamic recrystallization behavior of β−γ TiAl based alloy during high temperature deformation [J]. Intermetallics, 2018, 97: 52−57.

[12] SOKOLOVSKY V S, STEPANOV N D, ZHEREBTSOV S V, NOCHOVNAYA N A, PANIN P V, ZHILYAKOVA M A, POPOV A A, SALISHCHEV G A. Hot deformation behavior and processing maps of B and Gd containing beta-solidified TiAl based alloy [J]. Intermetallics, 2018, 94: 138−151.

[13] ZONG Ying-ying, WEN Dao-shen, GUO Bin, SHAN De-bin. Investigations of hydrogen-promoted α_2-lamella decomposition of a γ-TiAl based alloy [J]. Materials Letters, 2015, 152: 196−199.

[14] DEY S R, HAZOTTE A, BOUZY E. Crystallography and phase transformation mechanisms in TiAl-based alloys—A synthesis [J]. Intermetallics, 2009, 17(12): 1052−1064.

[15] SOKOLOVSKY V S, STEPANOV N D, ZHEREBTSOV S V, VOLOKITINA E I, PANIN P V, NOCHOVNAYA N A, KALOSHKIN S D, SALISHCHEV G A. The effect of Gd addition on the kinetics of $\alpha_2 \rightarrow \gamma$ transformation in γ-TiAl based alloys [J]. Intermetallics, 2020, 120: 106759.

[16] ZHANG Tian-long, WANG Dong, ZHU Jia-ming, XIAO Hu, LIU C T, WANG Yun-zhi. Non-conventional transformation pathways and ultrafine lamellar structures in γ-TiAl alloys [J]. Acta Materialia, 2020, 189: 25−34.

[17] XU Hao, LI Xiao-bing, XING Wei-wei, SHU Lei, MA Ying-che, LIU Kui. Phase transformation behavior of a Mn containing β-solidifying γ-TiAl alloy during continuous cooling [J]. Intermetallics, 2018, 99: 51−58.

[18] SCHWAIGHOFER E, CLEMENS H, MAYER S, LINDEMANN J, KLOSE J, SMARSLY W, GUETHER V. Microstructural design and mechanical properties of a cast and heat-treated intermetallic multi-phase gamma-TiAl based alloy [J]. Intermetallics, 2014, 44: 128−140.

[19] CHARPENTIER M, HAZOTTE A, DALOZ D. Lamellar transformation in near-γ TiAl alloys—Quantitative analysis of kinetics and microstructure [J]. Materials Science and Engineering A, 2008, 491: 321−330.

[20] XU Run-run, LI Miao-quan, LI Hong. Kinetic analysis and strain-compensated constitutive models of Ti−42.9Al−4.6Nb−2Cr during isothermal compression [J]. Progress in Natural Science: Materials International, 2020, 30(2): 260−269.

[21] XU Run-run, LI Hong, LI Miao-quan. Dynamic recrystallization mechanism of γ and α phases during the isothermal compression of γ-TiAl alloy with duplex structure [J]. Journal of Alloys and Compounds, 2020, 844: 156089.

[22] FULLMAN R L. Measurement of particle sizes in opaque bodies [J]. JOM, 1953, 5(3): 447−452.

[23] CHEN Hui-su, SUN Wei, STROEVEN P, STROEVEN M. Stereological method of calculating the average value of surface spacing between the neighboring aggregate grains in concrete [J]. Journal of Harbin institute of Technology, 2005, 37(11): 1511−1514. (in Chinese)

[24] SHECHTMAN D, BLACKBURN M J, LIPSITT H A. The plastic deformation of TiAl [J]. Metallurgical Transactions, 1974, 5(6): 1373−1381.

[25] APPEL F, CLEMENS H, FISCHER F D. Modeling concepts for intermetallic titanium aluminides [J]. Progress in Materials Science, 2016, 81: 55−124.

[26] IMAYEV R M, IMAYEV V M, OEHRING M, APPEL F. Microstructural evolution during hot working of Ti aluminide alloys: Influence of phase constitution and initial casting texture [J]. Metallurgical and Materials Transactions A, 2005, 36(3): 859−867.

[27] XU Run-run, LI Hong, LI Miao-quan. Flow softening mechanism in isothermal compression of β-solidifying γ-TiAl alloy [J]. Materials & Design, 2020, 186: 108328.

[28] INUI H, TODA Y, YAMAGUCHI M. Plastic deformation of single crystals of a DO19 compound with an off-stoichiometric composition (Ti−36.5at.%Al) at room temperature [J]. Philosophical Magazine A, 1993, 67(6): 1315−1332.

[29] MINONISHI Y. Plastic deformation of single crystals of Ti3Al with D019 structure [J]. Philosophical Magazine A, 2006, 63(5): 1085−1093.

[30] SMALLMAN R E, NGAN A H W. Modern physical metallurgy [M]. 8th ed. Amsterdam: Elsevier, 2014.

[31] CERRETA E, MAHAJAN S. Formation of deformation twins in TiAl [J]. Acta Materialia, 2001, 49(18): 3803−3809.

双态组织 β 凝固型 γ-TiAl 合金的定量表征

胥润润，李淼泉

西北工业大学 材料学院，西安 710072

摘　要：显微组织调控对于金属材料的精确塑性成形极为必要，尤其是双态组织 γ-TiAl 合金。基于体视学原理，双态组织 γ-TiAl 合金高温塑性变形后的显微组织分为 β_0 晶粒、残余 α_2/γ 片层团、α_2 晶粒和 γ 晶粒 4 类结构单元。结果表明：随着变形程度的增大，γ-TiAl 合金高温塑性变形后 β_0 晶粒的体积分数略微增大，残余 α_2/γ 片层团和 α_2 晶粒的体积分数逐渐减小，而 γ 晶粒的体积分数逐渐从 64.39%增大至 78.47%。基于定量结果，深入研究 $\alpha\rightarrow\gamma$ 相变，证实高温塑性变形促进 $\alpha\rightarrow\gamma$ 相变。第一种 $\alpha\rightarrow\gamma$ 相变类似于台阶控制生长机制，残余 α_2/γ 片层团通过该种机制逐渐转变为 γ 晶粒；第二种 $\alpha\rightarrow\gamma$ 相变为 α/γ 相界面迁移机制。

关键词：TiAl 合金；体视学；数字图像分析；显微组织；相变

(Edited by Bing YANG)